THE ASTROPHYSICAL JOURNAL, 405:706–719, 1993 March 10


# AN *IRAS* SURVEY OF STAR-FORMING REGIONS TOWARD CYGNUS

STEN F. ODENWALD[1,2] AND PHIL R. SCHWARTZ[2]
*Received 1992 April 6; accepted 1992 September 15*


## ABSTRACT

The distribution of young stellar objects toward the Cygnus X region obtained from the *Infrared Astronomical Satellite* (*IRAS*) is combined with a recent $^{12}$CO ($J = 2$–1) survey. The most luminous young stellar objects (YSOs) are examined for membership in the Local arm and the Perseus arm. The far-infrared, radio, and molecular emission is also analyzed from a global perspective. Seventy YSOs have been identified, corresponding to stars earlier than ≈B7 ZAMS, primarily associated with molecular clouds in the Local arm. The $^{12}$CO ($J = 2$–1) emission associated with these YSOs reveals 23 instances of broad-line wings including 10 with spatially complex, extended high-velocity molecular emission.

We have identified a new Perseus arm star-forming region, IRAS 20144+3726, and have also identified 20264+4042 and 20321+4112 near the H II regions DR 7 and 18P61 as broad-wing outflow sources also located in the Perseus arm. We conclude that no more than three YSOs earlier than approximately B0 ZAMS currently exist in the Perseus arm region located behind Cygnus X. Although we find no compelling evidence in the large-scale far-IR emission confirming the existence of the so-called Cygnus Superbubble, the Cygnus OB 2 association, is found to coincide with a localized cavity in which some dust depletion has occurred.


*Subject headings:* infrared: stars — ISM: individual (Cyg X) — radio lines: stars — stars: formation — stars: pre–main sequence

## 1. INTRODUCTION

Cygnus X ($b^{II} = 75°$–$85°$) has long been recognized as one of the more structurally complex regions of the Galactic plane. Originally discovered as a single prominent, extended thermal radio source by Piddington & Minnett (1952), it was so named to distinguish it from the nearby, extragalactic source Cygnus A. As the resolutions of the surveys have continued to increase, so too have the number of detected sources, culminating in the study by Wendker (1984) in which nearly 800 discrete radio continuum peaks have been identified.

Although it is possible to obtain some limited consensus over the large-scale galactic features toward Cygnus X (Liszt 1985), kinematic distances to individual star-forming regions (SFRs) within these components are difficult to determine since their velocity differences are often comparable to the ±6 km s$^{-1}$ dispersion of clouds in the Galactic plane (Magnani, Blitz, & Mundy 1985). The Perseus arm can be traced as a nearly continuous feature through Cygnus by mapping the distribution of H II regions (Georgelin & Georgelin 1976) and luminous stars (Humphreys 1976). Beyond the Perseus arm, indications appear in the surveys by Davies (1957) and Simonson (1974) of additional high-velocity components that may correspond to even more distant spiral arms. The Sun is located on the inner edge of the so-called Local arm, an interpretation by Dickel, Wendker, & Bieritz (1970) and Bochkarev & Sitnik (1985) also consistent with the distribution of various spiral arm tracers reviewed by Schmidt-Kaler (1976) and Humphreys (1976) and models of the diffuse Galactic radio emission by Beuermann, Kanbach, & Berkhuijsen (1985).

Some progress has been made in determining the relative locations of at least the most luminous (SFRs). Recombination line studies by Reifenstein et al. (1970), Barcia et al. (1985), and Piepenbrink & Wendker (1988), for example, show that the majority of the SFRs have velocities similar to molecular material in the Local arm. Piepenbrink & Wendker (1988), Heske & Wendker (1985), and Landecker, Wendker & Higgs (1989) find that the most distant radio sources include a supernova remnant, CTB 87, and three H II regions DR 7, G80.35+0.73, and 18P61 all associated with the Perseus arm based on their large, negative velocities. No SFRs have thus far been identified with $-15 < V_{LSR}(\mathrm{km\ s^{-1}}) < -30$ suggesting that an "Interarm Gap" may exist between the Perseus arm and the Local arm. The Interarm Gap also appears to be devoid of molecular clouds according to Cohen et al. (1980).

The locations of the radio continuum and molecular cloud sources in the Local arm are only known with some accuracy for the small number that happen to coincide with optical landmarks such as the Cygnus OB2 association at 2100 pc, or nebulae such as IC 1318 ($d = 1500$ pc) and the complex near NGC 7000 at a distance of 500 pc (Wendker, Benz, & Baars 1983). According to Dickel, Wendker, & Bieritz (1969) and reviews by Bochkarev & Sitnik (1985), nearly all of the remaining optical nebulae in the field lie between 1.2 and 2.4 kpc. The survey by Cong (1977) identified 78 individual molecular clouds comprising approximately three major complexes with $-25 < V_{LSR}(\mathrm{km\ s^{-1}}) < +25$ and distances less than 3 kpc. The first group contains nearby objects at large, positive $V_{LSR}$, with $d(\mathrm{pc}) < 1500$ that appear to be associated with the Cygnus rift/Goulds Belt population including DR 17, W 75N, and S 106. The nearest clouds are illustrated in Figure 1 and are probably no more than 700 pc distant (Neckel & Klare 1980), establishing a relatively firm lower limit to the distances of the nearest star-forming molecular clouds toward Cygnus.

The second group at an intermediate distance between 1200 and 1500 pc includes the supernova remnant DR 4 and the H II regions DR 5, 6, 9, 12, and 13 with $-6 < V_{LSR}(\mathrm{km\ s^{-1}}) < -3$ situated near IC 1318 and Cyg OB 9 ($d = 1200$ pc). A third more distant group, DR 18, 21, 22, 23, and probably ON 2 with $V_{LSR} \approx -3$ to $-5$ km s$^{-1}$ and $d \approx 2000$ pc is located toward

[1] Applied Research Corporation, 8201 Corporate Drive, Suite 1120, Landover, MD 20785.
[2] NRL, Center for Advanced Space Sensing, Code 4138-S, Washington, DC 20375.

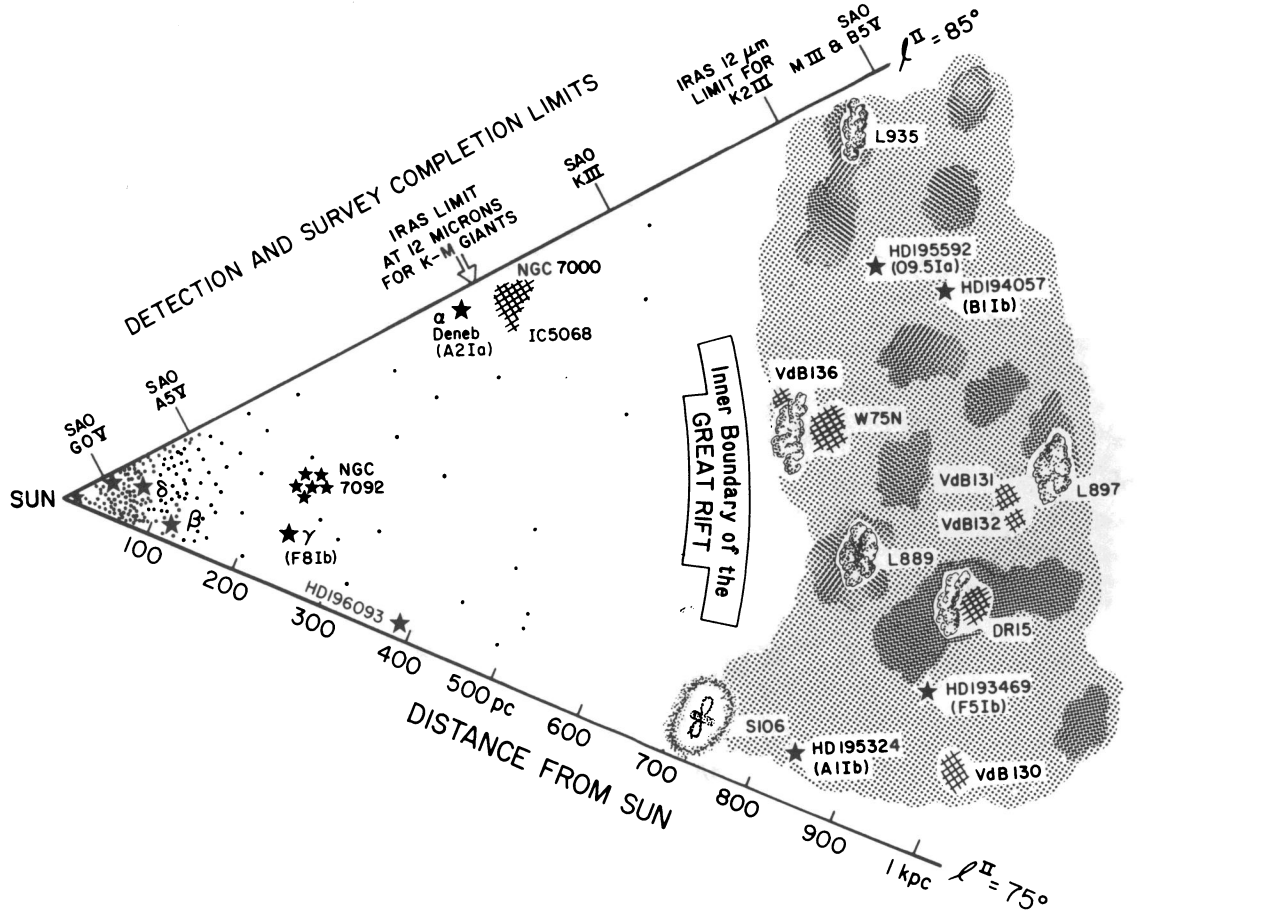


FIG. 1.—Principal star-forming regions within 1 kpc in the direction of Cygnus. Also shown is the limit of the Smithsonian Astrophysical Observatory star catalog for main-sequence stars later than A5, and the *IRAS* 12 μm limit for giant stars later than K2 III.

Cyg OB 1 and 2. In terms of their velocities, these two groups are indistinguishable and together constitute the majority of the CO emission and active, luminous SFRs toward Cygnus X.

Far-IR emission from Cygnus X has also been studied with balloon-borne telescopes by Hoffman, Frederick, & Emery (1971) and Campbell et al. (1980) from which as many as 49 pointlike (< 15′) sources could be discerned, most appearing to coincide with the brighter radio continuum features identified by Downes & Renhart (1966). Subsequent high-resolution (1′) studies by Odenwald et al. (1986, hereafter Paper I; 1990, hereafter Paper II) of several of the unresolved sources were able to show that DR 6, 7, 15, 20, and 22 were probably small colonies of two or more late-O or early B-type stars. The advent of the *Infrared Astronomical Satellite* (*IRAS*) has greatly enlarged these far-IR studies by simultaneously imaging both the extended and discrete sources toward Cygnus X. The *IRAS* Point Source Catalog (1988, hereafter PSC) and all-sky survey now permit a high sensitivity ($S > 0.2$ Jy) and moderately high resolution (1′–5′) study to be undertaken of young stellar objects (YSOs) and SFRs throughout the Cygnus X region. Odenwald (1989, hereafter Paper III) has begun such an investigation by identifying additional luminous YSOs in the region using the *IRAS* PSC.

Based on the ongoing discussion, Figure 2 summarizes the general distribution of SFRs toward Cygnus including both the Local arm and Perseus arm components. Some latitude has been exercised in representing the distribution of the interstellar medium and its structure, particularly in the Perseus arm where few large molecular clouds of the kind found in the Local arm have been detected.

The intimate association between YSOs and molecular clouds makes them a potentially far more accurate probe of Galactic structure than the optically identified OB stars. YSOs represent an "intermediate population" of spiral arm tracers between the molecular clouds and evolved OB stars, and may provide an important missing link between the models of Galactic structure revealed by these two common tracers. In this paper we will extend previous far-IR studies of the Cygnus X SFRs by examining the distribution of the *IRAS* point sources and extended far-IR emission and how they correlate with the other radio and molecular features in the region. These compact SFRs will be related to the large-scale distribution of molecular clouds and radio sources in the Local arm and the Perseus arm. We also describe a recent $^{12}$CO survey of the brighter YSO candidates to identify new outflow sources.

## 2. OBSERVATIONS

### 2.1. *Far-Infrared Emission*

The extended emission from Cygnus X has been mapped at 12, 25, 60, and 100 μm by the *IRAS* survey and appears in Single Hours Confirmed (HCON-1) Sky Image No. 044. These

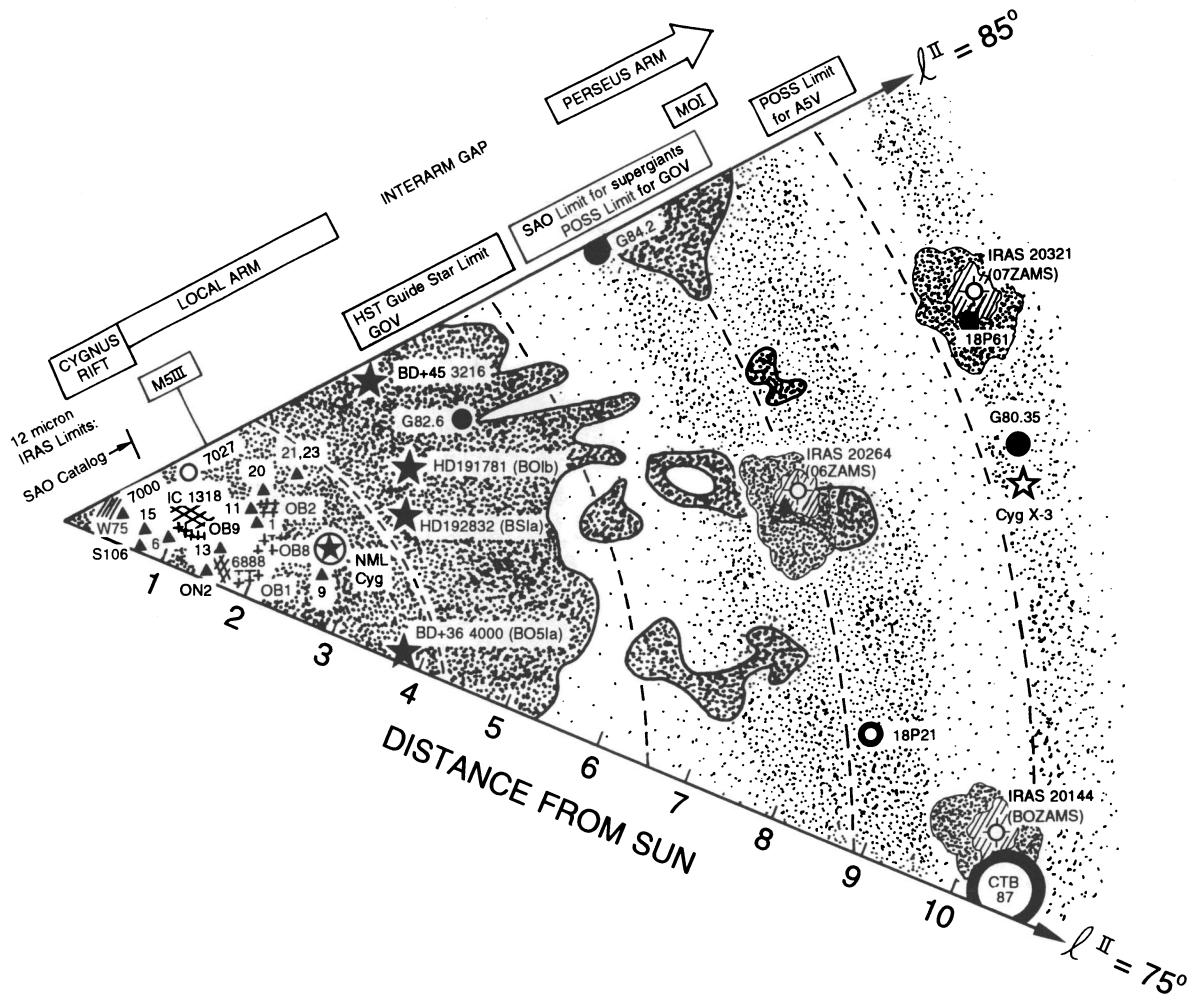


FIG. 2.—Approximate locations of star-forming regions toward Cygnus to a distance of 10 kpc. The plotted curved lines from left to right indicate the expected $V_{lsr}$ at 0, −20, −40, and −60 km s$^{-1}$ based on the rotation curve model described by Burton (1988). Radio sources identified by Downes & Rinehart (1966) indicated by numbered, filled triangles. NGC objects identified by four-digit numbers. Major OB associations indicated by crosses. The distribution of the molecular clouds is indicated by the shaded regions based on the CO survey by Leung & Thaddeus (1992). Location of the Perseus and Outer arms indicated by lighter shading based on the survey by Burton (1985). Also shown are the *Hubble Space Telescope* Guide Star Catalog limits for detection of main-sequence stars later than G0; the *IRAS* 12 μm brightness limit for M0 supergiants; and the Palomar Observatory Sky Survey limit for main-sequence stars later than A5.

data were obtained at spatial resolutions of 0.′75 × 4.′5 (12 and 25 μm), 1.′5 × 4.′7 (60 μm), and 3.′0 × 5.′0 (100 μm), with the sky images themselves gridded into 2′ × 2′ bins. No effort has been made to correct the images for instrumental artifacts (e.g., stripping and bright star hysteresis) since they do not interfere with the interpretation of the image data. The far-IR appearance of the Cygnus X field at 100 μm, along with the identification of the principal objects of interest, is shown in Figure 3.

The distribution of dust temperature and optical depth throughout the region is illustrated in Figures 4*a* and 4*b*, which have been extracted from the 60 and 100 μm flux measurements. Dust temperatures were obtained by computing the flux ratio $S(100\ \mu m)/S(60\ \mu m)$ at each image position and solving the Planck equation for the corresponding temperature, $T_d$, assuming that the far-IR emission is optically thin and that the dust grains follow the emissivity law $e(\nu) \propto \nu^{1.0}$. Optical depths at 100 μm were then determined by comparing the predicted blackbody surface brightness with the actual $S(100\ \mu m)$ measured by *IRAS*. These techniques for manipulating the *IRAS* sky flux data are described in more detail by Verter & Rickard (1992).

Information about the discrete source component presented in Tables 1 and 2 was extracted from the *IRAS* PSC, which lists 1700 sources detected in one or more of the *IRAS* bands in the region $20^h05^m < \alpha < 20^h45^m$ and $37°00' < \delta < 42°30'$. In regions not confused by the general diffuse background emission, the PSC is believed to be a complete survey of bright far-IR sources with sizes $\Theta < 5'$. Extended far-IR sources with sizes significantly greater than this are not included due to the criteria used to assemble the PSC (Beichman et al. 1985). The result is that luminous, extended SFRs such as DR6, DR7, or ON 2 do not appear in the catalog, although more compact YSOs associated with these SFRs should be present in the catalog.

### 2.2. $^{12}$CO ($J = 2$–1, *and* $J = 1$–0)

The $^{12}$CO ($J = 2$–1) observations were obtained at 230.538 GHz with the NRAO[3] 12 m telescope on Kitt Peak near

[3] The National Radio Astronomical Observatory is operated by Associated Universities for Research in Astronomy, Inc., under cooperative agreement with the National Science Foundation.

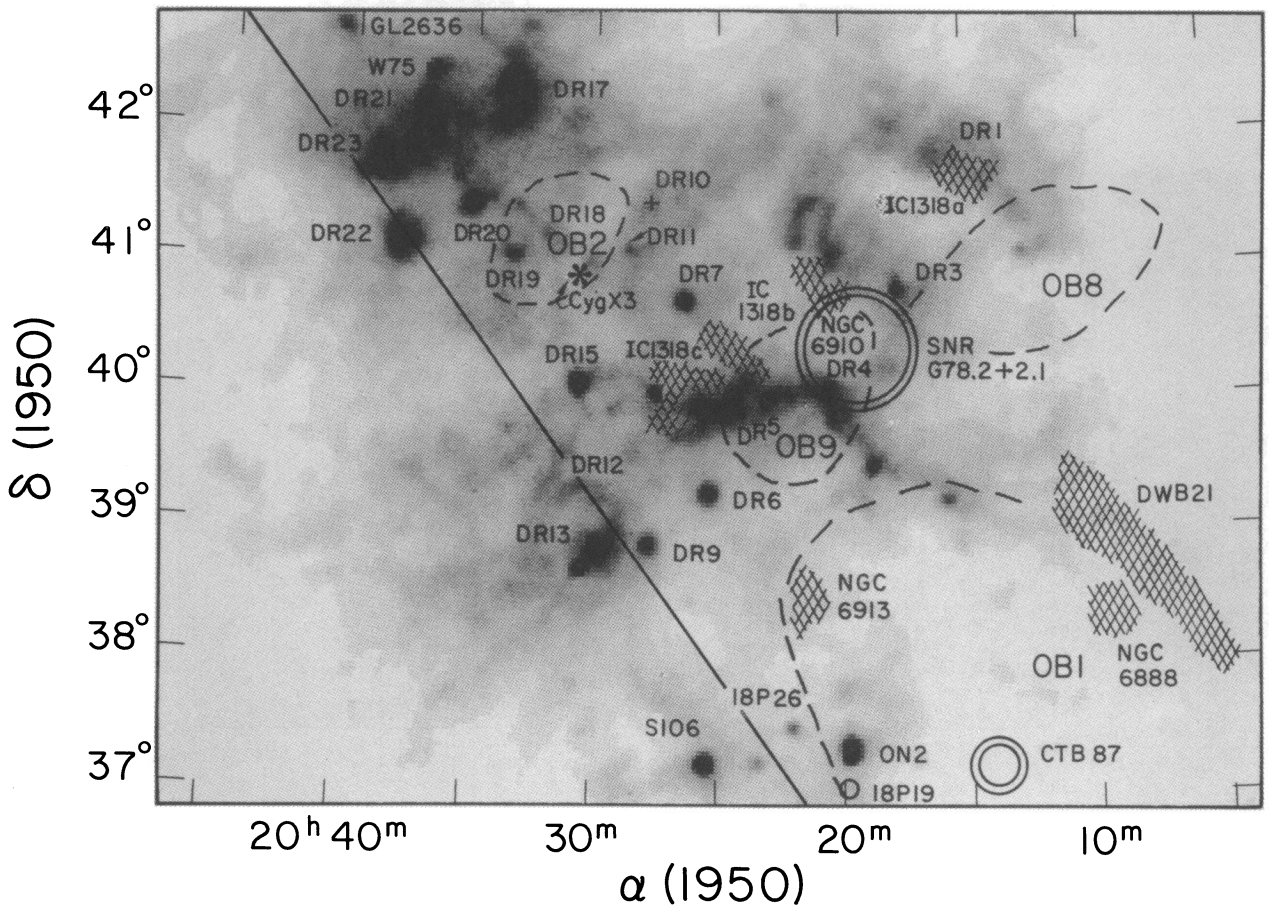


FIG. 3.—Principal objects in the field of Cygnus X superposed on an *IRAS* 100 μm gray-scale map of the region. *Crosshatched regions:* optical nebulosity; *Filled circles:* supernova remnants; *Dashed lines:* boundaries of major OB associations.

TABLE 1

STARLIKE OBJECTS WITH YSO CONTINUUA

| Name | Star |
|---|---|
| 20079+3747..... | DO 18645 |
| 20108+3852..... | SAO 69609 |
| 20144+4156..... | V396 Cyg |
| 20148+4043..... | SAO 49402 |
| 20155+4138..... | V437 Cyg |
| 20160+3911..... | RAFGL 2549 |
| 20163+4150..... | SAO 49439 |
| 20187+4111..... | LkHα 224 |
| 20197+3721..... | BC Cyg |
| 20198+3716..... | MWC 1015 |
| 20204+3752..... | AS 411 |
| 20212+3920..... | MWC 342 |
| 20215+4035..... | SAO 49563 |
| 20221+3726..... | RAFGL 5501S |
| 20242+4058..... | IRC 40416 |
| 20287+4020..... | DO 38486 |
| 20292+3829..... | DO 19082 |
| 20296+4048..... | AFGL 2600 |
| 20297+4052..... | Cyg II-13 |
| 20304+4059..... | Cyg II-10 |
| 20310+4029..... | MWC 349 |
| 20311+4110..... | ASS 21 |
| 20314+4106..... | DO 19128 |
| 20315+4048..... | SAO 49784 |
| 20327+4055..... | SAO 49823 |
| 20340+3807..... | DO 19175 |
| 20357+3742..... | DO 19210 |

Tucson, Arizona on 1988 December 1–4 and 1990 December 30. The first survey was conducted with the 250 and 500 kHz resolution filter banks of the 1.3 mm Schottky receiver operated in parallel, centered at $V_{LSR} = 0.0$ km s$^{-1}$, and with resolutions of 0.33 and 0.65 km s$^{-1}$ per channel, respectively. The beam size was measured using NGC 7027 and was found to have a full width at half-maximum (FWHM) of 36″. The telescope focus and flux calibration were checked periodically by using DR21 (OH) as a reference. The brightness data have been corrected for the forward scattering efficiency, $\eta_{fss} \approx 0.75$, and is given in terms of $T_R^*$ which is related to the brightness temperature via $T_B = T_R^* \eta_s^{-1}$ where $\eta_s$ is the source coupling efficiency. It is assumed that the source completely fills the beam at each map position so that $\eta_s = 1.0$.

Since most outflow sources often have structure at scales of a few arcminutes, the sources in Tables 2 and 3 were mapped in a 3 × 3 grid with 1′ offsets to cover the large-scale structure, followed by a 3 × 3 position grid with 15″ offsets to fully sample the emission near the far-IR peak. The mapping was performed using the absolute position switching mode with 1 minute integrations at each point followed by a measurement of a reference off-source position at $\alpha = 20^h28^m$ and $\delta = 38°00'$. This reference position showed no detectable $^{12}$CO emission to a limit of $T_R^* < 0.3$ K. A linear baseline was subtracted from each spectrum using the outer 30 channels of each filter bank to establish an off-line reference level. Line center velocity and FWHM estimates have uncertainties of ±0.4 km s$^{-1}$ based on

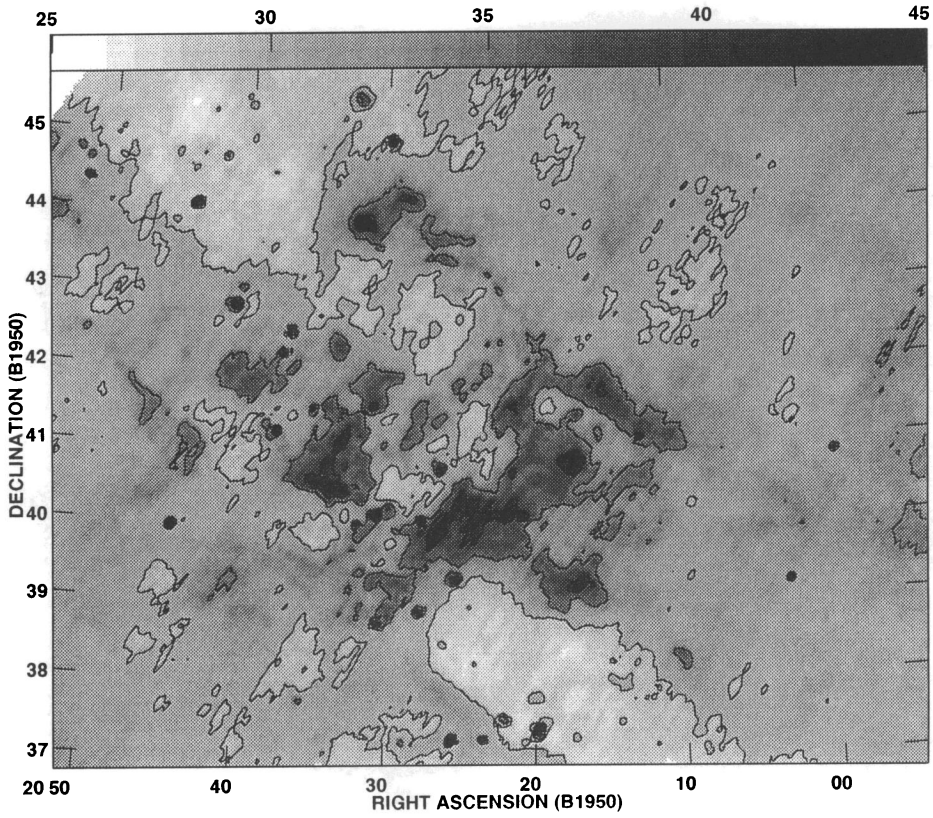


FIG. 4*a*

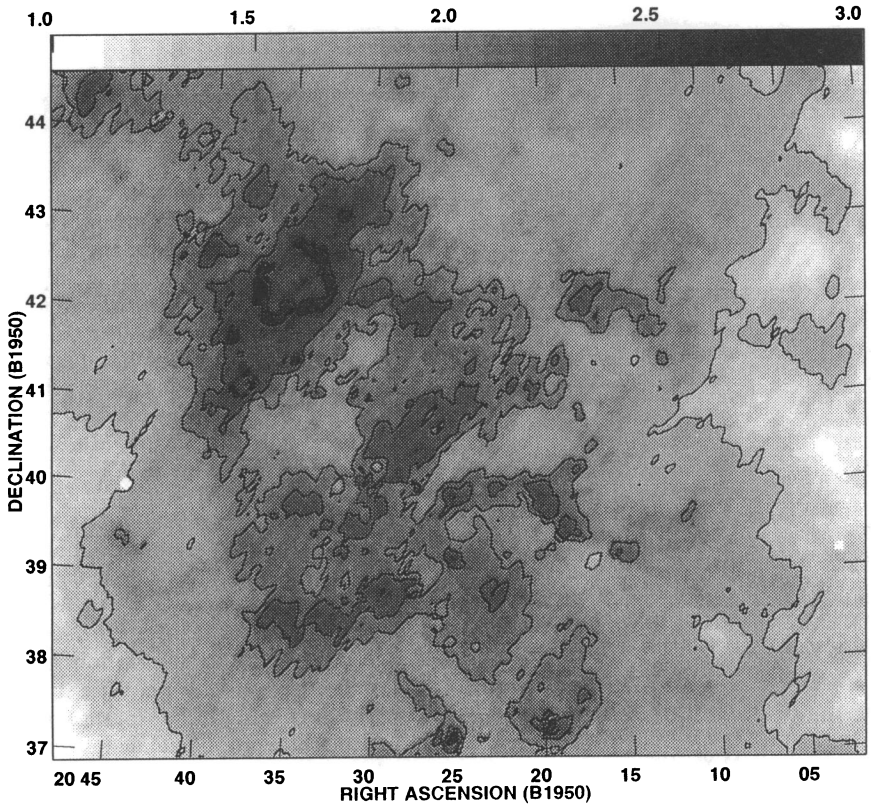


FIG. 4*b*

FIG. 4.—Dust temperature (*a*) and optical depth (*b*) distributions determined from the 60 and 100 $\mu$m *IRAS* images as described in § 2.1. Dust temperatures are indicated by the accompanying gray-scale wedge in units of K with contours at 30, 35, 40, and 45 K. Dust optical depth at 100 $\mu$m is given in logarithmic units in multiples of $10^{-5}$ nepers over the range from $10^{-5}$ to $10^{-2}$ nepers. Contours are presented at log ($N$) = 1.5, 2.0, 2.2, and 2.5 corresponding to $3.2 \times 10^{-4}$, $1.0 \times 10^{-3}$, $1.6 \times 10^{-3}$, and $3.2 \times 10^{-3}$ nepers.

TABLE 2

ESTIMATED PROPERTIES OF SURVEYED YSO CANDIDATES

| Name (1) | $\Theta_s$ (') (2) | $S_{100}$ (Jy) (3) | Log(F) ($W/m^2$) (4) | Log(L) ($L_\odot$) (5) | Log(L) ($L_\odot$) (6) | Radio ID (7) |
|---|---|---|---|---|---|---|
| 20135+4138 | 13 | 165.0 | -11.18 | 1.99 | 2.90 | Isolated |
| 20144+3726 | 8 | 168.4 | -11.06 | 2.10 | 4.41[a] | |
| 20152+3917 | 12 | 101.2 | -11.39 | 1.78 | 2.69 | Isolated |
| 20152+4104 | 5 | 204.4 | -11.09 | 2.08 | 2.99 | |
| 20153+3850 | 3 | 310.3 | -10.86 | 2.31 | 3.22 | |
| 20154+4202 | 6 | 115.5 | -11.34 | 1.83 | 2.74 | DR 1 |
| 20157+3854 | 5 | 196.5 | -11.09 | 2.07 | 2.99 | |
| 20173+3714 | 31 | 300.7 | -10.84 | 2.33 | 3.24 | Isolated |
| 20178+4047 | 5 | 2877.0 | - 9.68 | 3.49 | 4.40 | |
| 20184+4054 | 1 | 107.6 | -11.36 | 1.81 | 2.72 | |
| 20188+3928 | 5 | 1440.0 | - 9.98 | 3.18 | 4.10 | |
| 20190+4152 | 7 | 238.8 | -11.01 | 2.16 | 3.07 | |
| 20196+3702 | 2 | 140.3 | -11.09 | 2.07 | 2.99 | 18P19 |
| 20197+3745 | 2 | 122.8 | -11.18 | 1.99 | 2.90 | |
| 20205+3948 | 5 | 1337.0 | -10.14 | 3.02 | 3.94 | |
| 20215+3725 | 8 | 193.7 | -11.08 | 2.08 | 2.99 | 18P26 |
| 20216+4107 | 9 | 717.9 | -10.45 | 2.71 | 3.62 | |
| 20217+3947 | 5 | 277.0 | -10.86 | 2.30 | 3.21 | |
| 20220+3728 | 1 | 2131.0 | - 9.98 | 3.18 | 4.09 | 18P26 |
| 20226+4206 | 5 | 178.9 | -11.02 | 2.14 | 3.05 | |
| 20227+4154 | 2 | 460.8 | -10.62 | 2.54 | 3.46 | |
| 20228+4215 | 8 | 523.6 | -10.66 | 2.50 | 3.41 | |
| 20230+3845 | 8 | 105.4 | -11.36 | 1.80 | 2.71 | |
| 20236+4058 | 3 | 140.1 | -11.04 | 2.12 | 3.04 | |
| 20243+3853 | 3 | 225.9 | -10.97 | 2.19 | 3.11 | 18P33 |
| 20253+4134 | 2 | 174.4 | -11.16 | 2.00 | 2.91 | |
| 20255+3712 | 2 | 13130.0 | - 8.99 | 4.18 | 5.09 | S 106[1] |
| 20257+3943 | 3 | 215.2 | -11.03 | 2.13 | 3.04 | |
| 20261+3922 | 10 | 155.0 | -10.96 | 2.21 | 3.12 | DR 6[2] |
| 20261+3825 | 11 | 335.0 | -10.81 | 2.35 | 3.26 | Isolated |
| 20264+4042 | 0 | 4601.0 | - 9.66 | 3.50 | 5.56[b] | DR 7[3] |
| 20272+4021 | 0 | 455.9 | -10.67 | 2.49 | 3.40 | |
| 20275+4001 | 0 | 5721.0 | - 9.25 | 3.91 | 4.83 | GL 2591 |
| 20277+3851 | 2 | 3105.0 | - 9.73 | 3.43 | 4.34 | DR 9[4] |
| 20281+4038 | 8 | 304.5 | -10.86 | 2.31 | 3.22 | |
| 20281+4006 | 3 | 528.6 | -10.66 | 2.50 | 3.41 | |
| 20286+4105 | 0 | 1387.0 | -10.13 | 3.04 | 3.95 | 18P51 |
| 20290+4052 | 3 | 136.7 | -11.20 | 1.96 | 2.88 | |
| 20293+3952 | 7 | 916.5 | -10.14 | 3.02 | 3.94 | |
| 20293+4007 | 5 | 376.8 | -10.81 | 2.35 | 3.26 | |
| 20300+3847 | 0 | 1101.0 | -10.36 | 2.80 | 3.71 | DR 13[5] |
| 20300+3734 | 32 | 118.4 | -11.32 | 1.85 | 2.76 | Isolated |
| 20304+4059 | 2 | 802.1 | -10.50 | 2.66 | 3.57 | |
| 20306+3958 | 11 | 288.6 | -10.92 | 2.24 | 3.15 | |
| 20306+4005 | 2 | 10070.0 | - 9.23 | 3.93 | 4.85 | DR 15[6] |
| 20306+3749 | ... | 316.3 | -10.79 | 2.37 | 3.28 | |
| 20307+4015 | 8 | 107.9 | -11.32 | 1.84 | 2.75 | DR 15 |
| 20319+3958 | 7 | 1054.0 | -10.09 | 3.08 | 3.99 | G79.4-0.0 |
| 20321+4112 | 0 | 921.5 | -10.38 | 2.78 | 4.78[c] | 18P61 |
| 20324+4057 | 8 | 147.1 | -10.86 | 2.31 | 3.22 | Isolated |
| 20327+4120 | 10 | 634.5 | -10.54 | 2.62 | 3.54 | Isolated |
| 20332+4124 | 9 | 1376.0 | -10.12 | 3.04 | 3.64 | Isolated |
| 20333+4102 | 2 | 2472.0 | - 9.94 | 3.22 | 4.13 | DR 18[7] |
| 20337+4104 | 4 | 545.0 | -10.65 | 2.51 | 3.42 | DR 18 |
| 20338+3934 | 3 | 106.9 | -11.35 | 1.81 | 2.72 | |
| 20343+4129 | 7 | 1035.0 | -10.14 | 3.02 | 3.93 | |
| 20350+4126 | 0 | 3272.0 | - 9.82 | 3.35 | 4.26 | DR 20[8] |
| 20358+3931 | 5 | 169.8 | -11.18 | 1.99 | 2.90 | |
| 20444+3925 | 10 | 203.1 | -11.06 | 2.10 | 3.01 | Isolated |

NOTES.—Luminosity in solar units is based on a distance of 700 pc (col. [5]) and 2 kpc (col. [6]). Entries for Perseus arm sources assume distances of (a, c) 10 kpc and (b) 7.5 kpc. Additional names for identified radio sources: (1) 18P39; (2) 18P37; (3) 18P42, AFGL 2586; (4) 18P48, AFGL 2593; (5) 18P55, AFGL 4267; (6) 18P59, AFGL 2602; (7) 18P64; (8) 18P73, AFGL 2616.

Gaussian fits to the data. The peak $T_R^*$ is known to within $\pm 0.2$ K.

Additional observations in the $^{12}$CO ($J = 2$–1) line were obtained on 1990 December 30 using the newly commissioned, 1 mm SIS receiver, together with the 500 kHz and 1 MHz filter banks operating in parallel. The observations were carried out despite considerable overcast at the 12 m site, using position switch mapping of a 3 × 3 grid of beam positions centered on each of the *IRAS* sources, and using 1′ offsets between beam positions with a 30 s integration per point. Chopper vane calibration was performed only once per source, and a reference OFF position was measured after each map position, resulting in acceptably flat spectral baselines and a typical noise of $\pm 0.2$ K despite the inclement weather.

The relevant line parameters for the detected sources are presented in Tables 3, 4, and 5. In some instances, more than one velocity component was detected. We list, however, only the properties of the components believed to be directly associated with the far-IR source on the basis of the line brightness, or its variation with respect to the *IRAS* position.

## 3. RESULTS

### 3.1. *Extended Far-IR Emission*

The *IRAS* sky survey, along with the recent results from the *Cosmic Background Explorer* (Hauser 1990), and the *COS B* $\gamma$-ray survey described by Bloemen (1987), reveal Cygnus X as an isolated, bright, and nearly circular feature in the Galactic plane. The circular appearance of Cygnus X at X-ray wavelengths was originally interpreted by Cash et al. (1980) as evidence for a "superbubble" formed by supernovae. Piepenbrink & Wendker (1988) and Landecker, Wendker, & Higgs (1989) have challenged the supernova-driven superbubble hypothesis by not finding evidence in the velocity field of this region for systematic expansion, nor finding the requisite number of supernovae remnants that would be needed to produce the superbubble.

Abbot, Bieging, & Churchwell (1981) have suggested that the combined stellar winds from hot OB stars in the Cyg OB 2 association would be sufficient to create such a superbubble in a few million years, a proposal also advanced by Bochkarev & Sitnik (1985) a few years later. The integrated radio continuum characteristics of Cygnus X have also been compared by Baars & Wendker (1981) as equivalent to that of a giant H II region. We have integrated the far-IR emission from the region with a suitable background correction provided by a measurement of the off-source emission at $\alpha = 20^h45^m$ and $\delta = 37°00'$, and we obtain flux densities at 12, 25, 60, and 100 $\mu$m of 140, 270, 2100, and 4900 kJy, repectively. The integrated spectrum, increasing toward longer wavelengths, indicates that extensive dust temperature gradients are present throughout Cygnus X, possibly contributed by numerous SFRs embedded within the molecular clouds in this direction. The total far-IR luminosity can be estimated for a mean reference distance of 2 kpc using the relationship provided by Casoli et al. (1986) so that $F(\text{Cyg X}) = 2.4 \times 10^{-7}$ W m$^{-2}$, yielding a luminosity of $3 \times 10^7 L_\odot$.

The mean equivalent spectral type of the 800 radio sources detected by Wendker (1984) is similar to that of H II regions powered by individual B0 ZAMS stars. The linear extent of Cygnus X as a single giant H II region is approximately 350 pc on the sky. In comparison with known giant H II regions such as W49 with $L = 2 \times 10^7 L_\odot$ and a diameter of 150 pc, Cygnus X would rank as one of the most luminous giant H II regions in the Galaxy if the interpretation by Abbott et al. (1981) were correct. This would require that the distances to the numerous H II regions, molecular clouds, and OB associations were consistent with a common distance, and with distance uncertainties comparable to the size of the giant H II region. This possibility appears to be excluded on the basis of the quality of the various distance estimates themselves whose individual uncertainties are in many instances nonoverlapping.

In addition to its large-scale circular appearance, the extended far-IR emission shows considerable internal structure. As indicated in Figure 3, the most prominent discrete far-IR sources in the field are the luminous radio sources identified by Downes & Rinehart (1986) which are primarily young OB associations. An *S*-shaped feature we will henceforth refer to as the Cygnus ridge also dominates the emission at all wave-

TABLE 3

ADDITIONAL SOURCES SURVEYED

| Name (1) | $\Theta_s$ (2) | $S_{100}$ (Jy) (3) | log ($F$) ( W m$^{-2}$) (4) | log ($L$) ($L_\odot$) (5) | $V_{LSR}$ (km s$^{-1}$) (6) | $T_R^*$ (K) (7) | $\Delta V$ (km s$^{-1}$) (8) | Comments (9) |
|---|---|---|---|---|---|---|---|---|
| 20099+3640..... | ... | 270.2 | −10.82 | 3.26 | ... | ... | ... | No CO |
| 20103+3633..... | ... | 273.3 | −10.88 | 3.20 | ... | ... | ... | No CO |
| 20116+3605..... | .. | 264.7 | −10.60 | 3.42 | +1.7 | 2.7 | 4.6 | +8.1, +5.0, −1.9 |
| 20138+3632..... | ... | 194.6 | −11.03 | 3.05 | −2.2 | 11.6 | 3.9 | Paper IV |
| 20160+3636..... | ... | 1161.1 | −10.19 | 3.89 | +0.3[a] | 10.4 | 7.3 | S 104, +6.3, −4.9 |
| 20216+4319..... | 15′ | 47.7 | −11.71 | 2.37 | ... | ... | ... | No CO, Isolated |
| 20219+4256..... | 2 | 126.0 | −11.29 | 2.79 | +2.9 | 4.0 | 9.9 | Broad wing |
| 20254+4347..... | ... | 146.6 | −11.19 | 2.89 | +4.6 | 2.4 | 4.6 | Isolated |
| 20406+4555..... | ... | 436.0 | −10.63 | 3.45 | ... | ... | ... | No CO |
| 20444+4629..... | ... | 239.8 | −10.79 | 3.29 | −3.9 | 9.4 | 5.4 | |
| 20446+4613..... | ... | 257.4 | −10.90 | 3.18 | ... | ... | ... | No CO |

[a] Broad wing source with $I_{red}$ = 27.3 K km s$^{-1}$ and $I_{blue}$ = 36.9 K km s$^{-1}$. Luminosities in col. (5) are estimated for a distance of 2 kpc.

lengths, with the brightest section extending east to west near $20^h24^m$ and 39°45′ containing the SFRs DR 5 and DR 15.

When compared with the molecular cloud distribution, some elements of the far-IR emission can be attributed to specific velocity features identified by Cong (1977). As noted by Campbell et al. (1980) and Campbell, Hoffmann, & Thronson (1981), the Cygnus ridge does follow a major molecular cloud complex mapped by Cong (1977) whose dense material can be traced to the nearby nebula IC 1318, bisecting it into IC 1318b and IC 1318c. The majority of the Cygnus ridge seen at far-IR wavelengths is, therefore, associated with foreground molecular clouds nearer than 1500 pc. Much of the western region, for example, follows the distribution of the cloud component for which $-8 < V_{LSR}(\text{km s}^{-1}) < 0$. This component coincides with the Cygnus ridge including the DR 1, 13, S106, and ON2, as well as the majority of the emission in the vicinity of DR 20. The correspondence between the far-IR emission and molecular material between $0 < V_{LSR}(\text{km s}^{-1}) < +8$ is nearly as good and coincides with emission near DR 15, the extension of the Cygnus ridge near $20^m + 39°$, and the central Cygnus ridge component near $20^h20^m + 41°$. Beyond this simple decomposition, however, the assignment of the extended far-IR emission to specific molecular cloud subcomponents toward Cygnus cannot be made reliably.

TABLE 4

YSO CANDIDATES WITHOUT SIGNIFICANT BROAD WINGS

| Name (1) | $V_{LSR}$ (km s$^{-1}$) (2) | $T_R^*$ (K) (3) | $\Delta V$[a] (km s$^{-1}$) (4) | Comments (5) |
|---|---|---|---|---|
| 20135+4138..... | 3.9 | 1.1 | 6.5 | One position only |
| 20144+3726..... | −57.2 | 2.2 | 3.9 | −71.5, +11.7 |
| 20152+3917..... | +2.0 | 10.9 | 8.5 | +3.9 |
| 20152+4104..... | +6.6 | 19.6 | 2.0 | Paper IV, +11.2 |
| 20154+4202..... | −3.3 | 6.7 | 3.0 | |
| 20153+3850..... | +2.0 | 20.0 | 4.5 | |
| 20157+3854..... | +2.2 | 13.2 | 1.8 | Paper IV |
| 20178+4047..... | +0.7 | 29.6 | 5.9 | −3.6 |
| 20184+4054..... | +2.6 | 5.8 | 2.8 | +9.1, −3.9 |
| 20196+3702..... | −5.0 | 3.4 | 3.3 | One position only |
| 20197+3745..... | −2.6 | 1.2 | 3.5 | −26.0 |
| 20205+3948..... | −2.3 | 22.0 | 6.6 | |
| 20216+4107..... | −2.6 | 15.2 | 5.6 | +10.4 |
| 20217+3947..... | −2.3 | 14.4 | 3.6 | 0.0 |
| 20226+4206..... | +4.6 | 19.5 | 6.5 | |
| 20230+3845..... | +5.9 | 14.3 | 9.8 | Blend w/+3.5, 0.0 |
| 20236+4058..... | 0.0 | 15.8 | 2.1 | Paper IV |
| 20243+3853..... | +8.4 | 7.0 | 6.3 | +0.7 |
| 20253+4134..... | +3.3 | 8.1 | 3.9 | |
| 20261+3922..... | −0.7 | 4.3 | 4.6 | −4.6 |
| 20281+4038..... | +11.7 | 6.4 | 10.4 | +3.9, −3.5 |
| 20286+4105..... | −4.6 | 24.7 | 6.3 | Paper IV; +11.3 |
| 20293+3952..... | −1.7 | 9.6 | 7.3 | Paper II; +9.9, +13.2 |
| 20300+3734..... | 0.0 | 10.0 | 5.2 | |
| 20300+3847..... | +2.0 | 15.0 | 7.1 | 13, −6.5 |
| 20304+4059..... | −11.0 | 17.0 | 6.5 | |
| 20306+3958..... | +3.6 | 6.9 | 3.3 | +5.6, +7.6 |
| 20307+4015..... | 0.0 | 3.4 | 5.6 | +9.1 |
| 20319+3958..... | +8.5 | 12.0 | 7.8 | −4.0 |
| 20327+4120..... | +5.8 | 14.5 | 8.5 | −3, −29.7, −32.3 |
| 20337+4104..... | +7.1 | 15.0 | 4.6 | −2.8 |
| 20338+3934..... | +10.4 | 3.7 | 4.9 | −2.0, −6.0 |
| 20343+4129..... | +11.4 | 28.2 | 7.3 | Paper II; −0.7 |
| 20350+4126..... | −2.6 | 11.6 | 7.8 | 0.7, 6 |
| 20358+3931..... | +6.5 | 10.1 | 7.2 | +13.7, −2.0 |

[a] Line widths given in km s$^{-1}$ and estimated at 500 mK.

The Cygnus ridge is most likely internally heated by nascent OB associations such as DR 1, 13, and 15 that are now forming in the molecular clouds in the velocity range from $-8 < V_{LSR}(\text{km s}^{-1}) < +8$. As noted by Landecker et al. (1989), the thermal radio emission from Cygnus X follows the distribution of the far-IR emission and is brightest at locations corresponding to these luminous H II regions. This intimate relationship between the far-IR and radio continuum ridge and the prominent H II regions also follows from a comparison of the 100 $\mu$m emission and the dust temperature distribution shown in Figure 4*a*. The Cygnus ridge is clearly a local temperature maximum in the region with $38 < T_d(\text{K}) < 42$ and includes several "hot spots" for which $T_d > 43$ K associated with the individual H II regions. In addition to the Cygnus ridge, the dust temperature map also shows that considerable local heating occurs in the horseshoe-shaped region near DR 12, DR 13, DR 15, as well as in the vicinity of Cyg OB2.

A number of additional features can be identified in Figures 3 and 4. Two unusual arclike features can be identified in Figure 4. The first of these, Arc 1, appears as a temperature enhancement centered at $\alpha = 20^h26^m$, $\delta = +42°30'$ with a diameter of $\approx 1.°5$. A second arc, Arc 2, appears as a dust density enhancement in Figure 4*b* in the DR 21 region centered on $\alpha = 20^h35^m$, $\delta = +42°15'$ with a diameter of $\approx 1°$. Similar ridges have been described by Landecker et al. (1989); however, none of the ridges in their survey coincide with either

TABLE 5

BROAD WINGED SOURCES IN CYGNUS X

| Name (1) | $V_{LSR}$ (km s$^{-1}$) (2) | $T_R^*$ (K) (3) | $\Delta V$ (km s$^{-1}$) (4) | $I_{RED}$ (K km s$^{-1}$) (5) | $I_{BLUE}$ (K km s$^{-1}$) (6) | Comments (7) |
|---|---|---|---|---|---|---|
| 20173+3714..... | +2.0 | 16.4 | 5.2 | ... | ... | −23.4 |
| 20188+3928..... | +1.8 | 13.6 | 12.2 | 81.7 | 120.1 | −6 |
| 20190+4152..... | −3.7 | 19.0 | 5.9 | ... | ... | +13.2 |
| 20215+3725..... | −3.3 | 7.5 | 23.8 | ... | ... | |
| 20220+3728..... | −2.6 | 20.0 | 12.2 | 365.9 | 48.9 | |
| 20227+4154..... | +4.0 | 10.0 | 5.3 | 24.3 | 34.1 | +7.9, +10.2 |
| 20228+4215..... | +5.4 | 15.0 | 16.9 | 87.2 | 38.1 | +9.2 |
| 20255+3721..... | −1.2 | 24.0 | 24.0 | **** | **** | S 106, +4.3 |
| 20257+3943..... | −2.3 | 11.0 | 9.2 | ... | ... | −4.6 |
| 20264+4042..... | −42.9 | 12.8 | 9.1 | ... | ... | +5.2 |
| 20272+4021..... | +6.8 | 22.8 | 7.3 | 5.3 | 63.6 | −1.7 |
| 20275+4001..... | −4.6 | 15.6 | 24.7 | 46.6 | 72.8 | −10.4, +0.7 |
| 20277+3851..... | −3.9 | 13.0 | 9.1 | ... | ... | +13.0, 0 |
| 20281+4006..... | +7.3 | 18.4 | 7.3 | 93.0 | 85.8 | +10.8, −1.0 |
| 20290+4052..... | −3.3 | 5.8 | 12.0 | ... | ... | −21, −30, −43, −61 |
| 20293+4007..... | −2.0 | 7.4 | 5.6 | ... | ... | +10.7 |
| 20306+3749..... | −3.9 | 8.0 | 8.7 | ... | ... | 9 |
| 20306+4005..... | +3.9 | 21.6 | 14.5 | 121.0 | 246.0 | Paper II, −1.4 |
| 20332+4124..... | −1.3 | 13.0 | 11.0 | ... | ... | +4.6, −30.6 |
| 20333+4102..... | +8.5 | 23.5 | 9.1 | ... | ... | |
| 20444+3925..... | −4.6 | 12.8 | 8.2 | ... | ... | −11.5 |

NOTE.—Wing emission from S 106 indicated by asterisks was detected but not mapped since it is a well-known outflow source. Line width given in col. (4) was estimated at the 500 mK level of the line profile.

of these two arcs. Arc 2 within DR 21 may be a young shell of compressed gas and dust recently produced by the expanding ionization front from this young OB association.

The majority of the extended dust emission detected between 60 and 100 $\mu$m not directly associated with the Cygnus ridge is produced by dust grains with $T_d = 28 \pm 5$ K somewhat warmer than the temperature range for "cirrus" material heated by the diffuse Galactic UV radiation field. The origin of this heating for the diffuse dust component cannot be the embedded OB stars responsible for the Cygnus Ridge since the local opacity is too large for the UV radiation from these stars to travel more than a few parsecs from their origin. Substantial numbers of OB stars exist, however, in the Cyg OB1, 2, 8, and 9 associations whose distances are in the range $1200 < d(\mathrm{pc}) < 2100$ (Alter, Balazs, & Ruprecht 1970; Reddish, Lawrence, & Pratt 1966). The local optical extinction toward these associations is $A_v < 1$ mag (Dickel & Wendker 1978) which allows the individual stars to be directly observed at these distances. These luminous stars are very likely the major source of dust grain heating for the extended far-IR component.

### 3.2. *The Cygnus OB2 Region*

As shown in Figure 4*b*, the Cygnus OB2 association near $20^h30^m + 40°.5$ corresponds to a minimum in the dust opacity. It is also coincident with a "hole" in the CO emission between $-8 < V_{LSR}(\mathrm{km\ s^{-1}}) < 0$ mapped by Cong (1977). At a distance of 2100 pc Cyg OB2 contains some of the most luminous stars in the Galaxy (Abbott et al. 1981). The failure to find any evidence for H II regions associated with the Cyg OB2 stars has suggested that the enormous quantities of Lyman continuum photons with $U \approx 275$ pc cm$^{-2}$ are freely escaping from the stars into the surrounding ISM. The resulting UV radiation field would be sufficient to photoionize all atomic hydrogen within 15 pc ($\approx 0°.4$) of the OB association if $n_H < 27$ cm$^{-3}$ (Huchtmeier & Wendker 1977). This also would result in $M_{H\,II} \approx M_{gas}$. Such a diffuse H II region does, in fact, coincide with the extended radio source discovered by Wendker (1970) at this location. In an environment containing such a luminous UV radiation field as the OB2 association, it is appropriate to ask whether some modification in the dust properties has occurred. Indeed as shown in Figure 4*b*, this radio source also coincides with a region of low far-IR emissivity and high dust temperature between 60 and 100 $\mu$m.

It has been suggested by Reddish (1967) and Elsasser & Voelcker (1974) that the dust component within Cyg OB2 may be enhanced relative to the gas component. The dust mass determined from stellar optical extinctions corresponded to $M_d \approx 100\ M_\odot$, while the gas component required to produce the extended H II region was estimated to be $M_{H\,II} \approx 10^3\ M_\odot$. Since it was presumed that $M_{H\,II} \approx M_g$, the resulting $M_g/M_d \approx 10$ was found to be substantially lower than the canonical ISM value of 100, leading to the proposal that the dust component is overabundant toward Cyg OB2. The current far-IR measurements, in fact, show that significantly less dust is present in this region than estimated using stellar extinction.

The *IRAS* data provide a direct measure of the total mass in the dust grain component emitting between 12 and 100 $\mu$m within Cyg OB2. The dust mass may be estimated from Campbell et al. (1980) and Hauser et al. (1984) as

$$M_d = \frac{\tau(\lambda)\Omega d^2}{K(\lambda)},$$

where $K(\lambda)$ is the dust mass absorption coefficient in cm$^2$ g$^{-1}$, $\tau(\lambda)$ is the far-IR optical depth, $\Omega$ is the solid angle of the emitting region, and $d$ is the distance to the source. Adopting $K(300\ \mu\mathrm{m}) = 4.6$ cm$^2$ g$^{-1}$ as suggested by Hauser et al. (1984) and $K(\lambda) \propto \lambda^{-2}$ for $\lambda \geq 100$ $\mu$m, one obtains for $d = 2$ kpc and $\Omega = 1.5 \times 10^{-4}$ sr that $M_d = 7.4 \times 10^3 \tau(100\ \mu\mathrm{m})\ M_\odot$. The estimated dust mass corresponding to the mean opacity of the

region of $\tau(100\ \mu m) = 1.0 \pm 0.3 \times 10^{-3}$ is, therefore, $M_d = 7.4 \pm 2.4\ M_\odot$, so that $M_g/M_d = 135 \pm 50$.

The 60 and 100 $\mu$m *IRAS* data are known to be at variance with the *COBE* data on the extended far-IR background, in that the *IRAS* flux measurements in these bands are a factor of 2 higher than measured by *COBE* (H. Moseley 1992, private communication). This will not greatly affect the derived dust color temperature deduced from the 60 and 100 $\mu$m data, but will affect the estimate for $\tau_{100}$ by overestimating $S(100\ \mu m)$ and therefore $\tau_{100}$ about a factor of 2. When corrected for this calibration difference between *IRAS* and *COBE*, we deduce that $M_d = 3.7 \pm 1.2\ M_\odot$, and $M_g/M_d = 270 \pm 100$.

Based on the *IRAS* data, the central core of Cyg OB2 is a region in which some change is apparent in the abundance of dust grains relative to the general interstellar medium. The associated $M_g/M_d$ is significantly higher than the interstellar average of 100. This suggests that fewer dust grains are present in this region than in the average ISM.

## 4. THE POINT SOURCE SURVEY

The Cygnus X field defined by the coordinate boundaries shown in Figure 3 contains 1700 sources in the *IRAS* PSC. Many of these can be expected to be nearby stars that will reveal nothing of the distribution of the molecular clouds in the direction of Cygnus. Only OB-type YSOs associated with the molecular clouds in this direction will be useful probes of this deep structure. It is unavoidable in a survey of this kind, that foreground stars and distant galaxies will be included which in many instances also resemble YSOs in the infrared. In Paper III we concluded that the number of galaxies mistaken for bright YSOs toward Cygnus X with $S(100\ \mu m) > 10$ Jy must be small, and of order unity.

The contribution to the survey by evolved late-type stars poses a far greater source of uncertainty in creating a complete flux-limited catalog of YSO candidates than background galaxies. Approximately $\frac{2}{3}$ of the sources in the PSC are known to be stars (Habing 1986) with $S(12\ \mu m) > S(25\ \mu m)$, and in the Cygnus X region, 403 of the point sources satisfied this minimal requirement. An additional 268 sources were detected at only 12 $\mu$m and we have also classified these as stellar sources. Collectively, these 671 candidates, comprising 40% of the sample, include 91 known cataloged stars primarily associated with stars in the Smithsonian Astrophysical Observatory catalog. The preponderance are K, M, and carbon stars with approximately equal numbers of giants and supergiants.

Some late-type stars, in particular OH/IR stars such as OH 17.7−2.0 (Olnon et al. 1984), are known to have strong IR excesses resembling YSOs at long wavelengths due to the reradiation of their photospheric emission by dust grains. The 27 sources in Table 1 had YSO-like continuua with $S(12\ \mu m) < S(25\ \mu m)$, but coincided with apparently stellar objects in the PSC. Six of these, SAO 49402, 49439, 49823, 6990, 6906 and V396 Cygni, were specifically identified in the PSC as late-type stars; moreover, the *IRAS* Atlas of Low Resolution Spectra (1986, hereafter the Atlas) also classified the IR spectra of 20242 and 20296 as being similar to those of late-type stars with carbon or oxygen-rich envelopes. We also note that five of the objects are B-type stars (SAO 49563, LkH$\alpha$ 224, IRC 40430, 40416, and MWC 349). Undoubtedly, the objects in Table 1 include many examples of OH/IR late-type stars, or OB stars with circumstellar dust emission. Since Zuckerman & Dyck (1986) and Zuckerman, Dyck, & Claussen (1986) have shown that OH/IR stars can also be detected via their $^{12}CO$ emission, these objects may, in the future, be useful probes of the distance-velocity relation toward Cygnus X.

### 4.1. *YSO Candidates*

The remaining 666 point sources toward Cygnus X were detected in at least two *IRAS* bands but failed the test for purely stellar continua between 12 and 25 $\mu$m since they may have had (1) only an upper limit established for the 12 $\mu$m emission (178/666); (2) a measured 12 $\mu$m flux density, but only a 25 $\mu$m upper limit (78/666); or (3) valid measurements at 12 and 25 $\mu$m but where $S(12\ \mu m) < S(25\ \mu m)$ (410/666). The least ambiguous YSO identifications occur for the subset of the third group consisting of 132 sources with fluxes measured in all four *IRAS* bands. Without exception, their monotonically increasing flux densities toward 100 $\mu$m follow the predicted pattern for YSOs (Shu, Adams, & Lizano 1987). These "first-ranked" YSO candidates, as we shall henceforth refer to them, are among the brightest 100 $\mu$m sources in the survey. For the purposes of this study, we consider only those 59 YSOs listed in Table 2 with $S(100\ \mu m) > 100$ Jy, a subset which substantially overlaps the group of bright YSOs described in Table 1 of Paper III. Also shown in Table 3 are additional far-IR sources that were surveyed, but which did not satisfy the selection criteria for the first-ranked sources.

The first-ranked YSOs in the field as shown in Figure 5 are preferentially found in regions where the extended thermal radio emission mapped by Wendker (1984) is brightest. The most active-star-forming regions appear to be associated with DR 3, DR 15, ON 2, and Cyg OB2. In a region as complex as Cygnus X some care must be exercised in assigning specific radio peaks to individual YSOs, particularly in view of the large beam widths employed in both the radio ($\Theta_r \approx 2'.6$) and far-IR ($\Theta_{ir} \approx 5'$) surveys, and the areal density of sources in the field. In Tables 2 and 3, we have used the radio source catalog by Landecker et al. (1989) along with a direct study of the 4.8 GHz maps by Wendker (1984) to identify the nearest prominent sources to each of the YSOs. All of the radio peaks found near the *IRAS* position are listed in Table 2 (col. [7]) and 3 (col. [9]), as well as the angular separation, $\Theta_s$, between the *IRAS* and radio positions in column (2). Individual radio source sizes estimated from the radio map were indeterminate due to the complex nature of the extended background emission; however, the typical size of relatively isolated sources was found to be $\Theta_{rs} \approx 8'$. The separations shown in Tables 2 and 3 are, therefore, well within the simple confusion scale defined by the mutual beam resolution $\Theta_c = (\Theta_r^2 + \Theta_{ir}^2)^{1/2} \approx 6'$, and its convolution with the typical radio source size $\Theta_c' = (\Theta_c^2 + \Theta_{rs}^2)^{1/2} \approx 10'$. Evidently, the first-ranked YSOs in Table 2 are adjacent to known, luminous radio sources toward Cygnus X, and as such are either the far-IR counterparts to the OB stars producing the H II regions, or radio-quiet B stars recently formed in the vicinity of active SFRs.

### 4.2. *Far-IR Properties*

In addition to their global distribution, as a population, additional physical properties of the sources can be estimated by fitting the continua using a simple two-temperature, optically thin dust model defined by

$$S(\nu) = A_H \nu^\beta B(T_H, \nu) + A_C \nu^\beta B(T_C, \nu)\,, \qquad (1)$$

where $\nu$ is the frequency corresponding to the effective wavelengths of each *IRAS* band. The subscripts $H$ and $C$ refer to the "hot" and "cold" dust components. Following the discussion

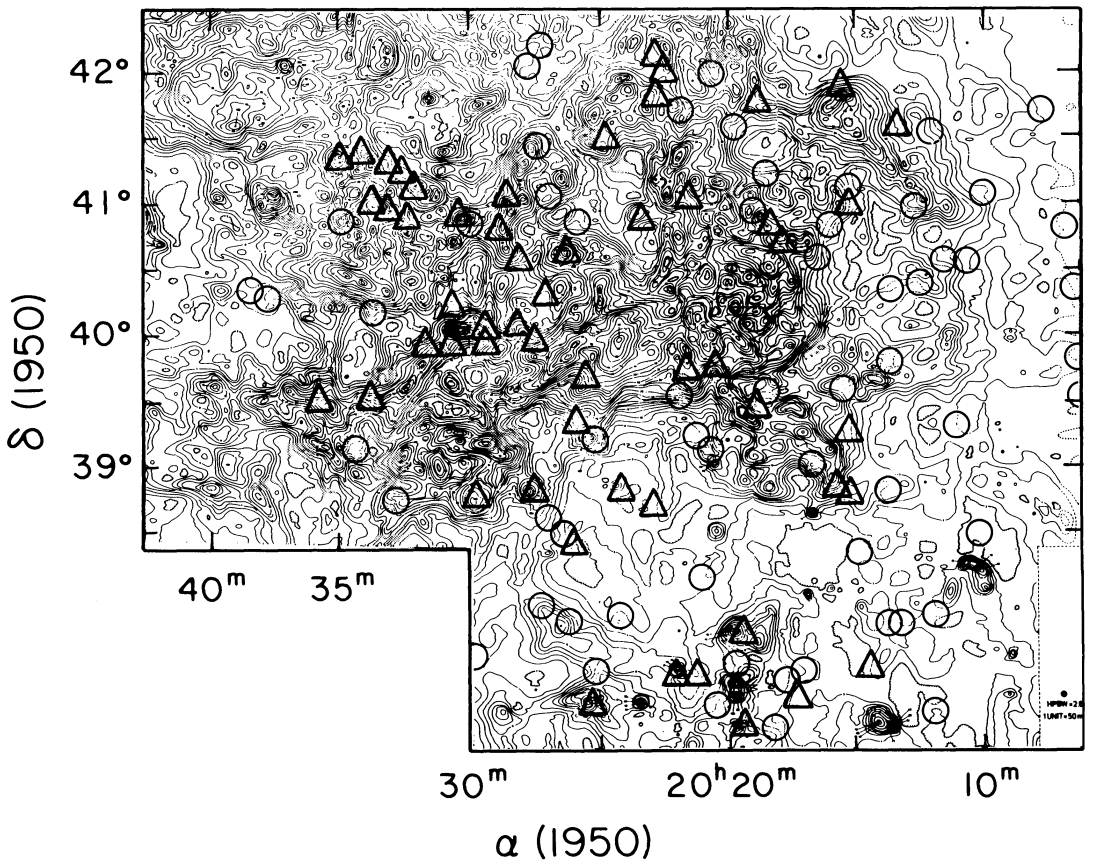


FIG. 5.—Locations of the 132 first-ranked YSO candidates as compared to the locations of the radio continuum features identified by Wendker (1984). *Triangles:* YSOs listed in Tables 2 and 3 with $S(100\ \mu m) > 100$ Jy; *Circles:* remaining first-ranked YSO candidates with 100 $\mu$m flux densities in the range $10 < S(\text{Jy}) < 100$.

in the *IRAS* Explanatory Supplement (1988), a color correction has been applied to the *IRAS* flux densities, $S(\nu)$, suitable for a $\beta = 1$ spectrum as indicated in the Supplement. Since the number of unknowns match the number of spectral measurements, the far-IR continuum fits are exact, and for the ensemble in Table 2 yield $T_c = 33 \pm 6$ K, and $T_h = 157 \pm 33$ K. The extended cold components account for greater than 80% of the total luminosity. Since $A_{H,C}\nu^{\beta} = \Omega_g \tau$ where $\Omega_g$ is the physical solid angle subtended by the region, for optical depths near unity we see that the YSOs have angular scales $(\Omega)^{1/2} \approx 60''$. This lower limit is already consistent with the pointlike character of these sources in the far-IR, compared to the *IRAS* detector beam profiles, suggesting that the YSOs are probably not objects for which $\tau \ll 1$.

By integrating equation (1), one may obtain the total flux radiated by each component, $F_{H,C}$, as a function of the two dust temperatures and effective solid angles,

$$F_i = A_i\left(\frac{2h}{c^2}\right)\left(\frac{k}{k}\right)^{4+\beta} T_i^{4+\beta}\Gamma(4+\beta)\zeta(4+\beta)\,, \qquad (2)$$

where $\Gamma$ and $\zeta$ are the gamma and Riemann zeta functions. Equation (2) may be evaluated to obtain $F_i = 6.86 \times 10^{17} A_i T_i^5$ W m$^{-2}$ listed in Tables 2 and 3 (col. [4]). The estimated far-IR luminosities in columns (5) and (6) have been determined from $L/L_{\text{sun}} = 3.0 F d_{\text{kpc}}^2$ assuming that the emission from the source is isotropic and where the total flux, $F$, is expressed in units of $10^{-13}$ W m$^{-2}$. This continuum-fitting method is superior to the one used in Paper III, yielding values for the total far-IR flux comparable to those obtained by Schwartz, Mozurkewich, & Odenwald (1990), who used a similar technique, and Casoli et al. (1986) in the specific case of S 106. The luminosities have been evaluated for two reference distances corresponding to the Cygnus rift (700 pc) in column (5), and the Local arm (2000 pc) in column (6), although 20144, 20264, and 20321 which are members of the Perseus arm have been assigned distances between 7 and 10 kpc.

According to Natta & Panagia (1977), the most luminous star in a given OB association will dominate the far-IR luminosity for reasonable choices of the cluster initial mass function. We therefore assume that the majority of the far-IR flux from a specific YSO originates in the earliest spectral type star consistent with the estimated far-IR luminosity. The far-IR luminosities span a range equivalent to stars from A0 to B0.5 ZAMS at 700 pc and B4-O7 ZAMS at 2 kpc. All of the YSOs coincident with the most luminous radio sources in Table 2 have $L > 3000\ L_{\odot}$, implying spectral types earlier than B2 ZAMS for individual stars. This is, in turn, consistent with their frequent association with radio sources since stars earlier than $\approx$B2 produce sufficient ionization to be readily detectable in this way.

The previous analysis assumes that the far-IR emission originates in an optically thin region possessing spherical symmetry. Although such models have been extensively investigated since the early 1970s, recent studies by Beckwith et al. (1990) suggest that for certain T Tauri stars, the IR and sub-

millimeter continua can be represented in terms of circumstellar disks that are optically thick for $\lambda < 100$ $\mu$m. Since some of the YSOs will be shown to have high-velocity outflows, we cannot dimiss such disklike geometries a priori. The emitted radiation from such a disk is readily determined from

$$S_\nu = 2\pi \int \theta B[\nu, T(\theta)]d\theta\,, \qquad (3)$$

with a disk temperature distribution given by $T(\theta) = T_0(\theta/\theta_0)^\alpha$ where $\theta_0$ and $T_0$ are the outer radius and temperature of the disk. We have solved such a disk model for the three quantities $\alpha$, $T_0$, and $\theta_0$ using the four *IRAS* flux measurements for each YSO in Table 2, and have found that the solutions generally yield the best fits for $\Theta_0 = 6''.4 \pm 2''.5$, $T_0 = 14 \pm 5$ K, and $\alpha = -0.5 \pm 0.1$.

At a mean distance of 2 kpc, $\Theta_0 \approx 13{,}000$ AU. Although the inferred linear extent of such a disk is large compared to known systems such as HL Tau or L1551, contamination of the YSO spectrum by cold molecular material can account for some of this discrepancy. If the *IRAS* beam intercepts a significant dust component radiating between 60 and 100 $\mu$m, the contribution by the disk at these wavelengths will be overestimated. The result is that $\Theta_0$ will also be an upper limit. The distribution of $\alpha$ suggests that these sources, as disklike systems, are more nearly characteristic of "accretion-phase" objects for which $\alpha \approx -0.5$, than the so-called "passive disks" for which $\alpha \approx -0.75$.

## 5. THE SPATIAL DISTRIBUTION OF THE SFRS

The $^{12}$CO spectra of each of the surveyed YSOs may be used to identify the $V_{LSR}$ of the associated molecular clouds, and from this to obtain an estimate for the kinematic distances to the YSOs. We have used the Galactic rotation curve model summarized by Burton (1988) based on $R_0 = 8.5$ kpc and $V_0 = 220$ km s$^{-1}$ to distinguish, where possible, between Local arm and Perseus arm SFRs. Representative loci of constant $V_{LSR}$ are indicated in Figure 3. Our $^{12}$CO survey of the 70 brightest YSOs toward Cygnus X, summarized in Figure 6, suggests that the majority are found in the same velocity range as the large-scale molecular cloud features primarily located within the Local arm.

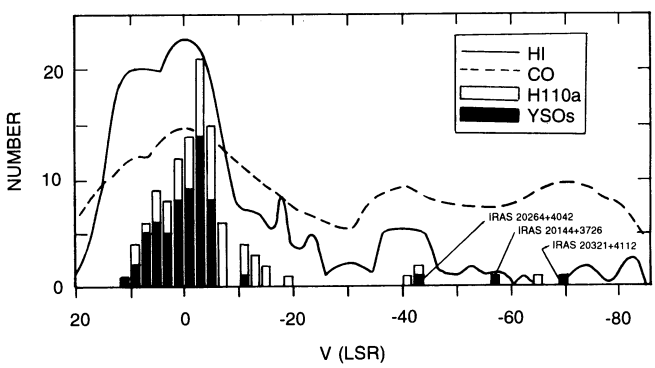


FIG. 6.—Histogram of the $^{12}$CO ($J = 2$–1) velocity components detected toward the YSOs surveyed in Tables 3 and 4 compared to other tracers of gas and molecular clouds within spiral arms. The "CO" curve indicates the velocities of peak CO emission adapted from the survey by Leung & Thaddeus (1992). The peak 21 cm emission of H I is based on the survey by Butler (1985). The H110-$\alpha$ sources identified in the histogram are those identified by Pipenbrink & Wendker (1988).

### 5.1. *The Perseus Arm*

Several YSOs have velocity components with $V_{LSR} < -20$ km s$^{-1}$ indicating possible membership in the Perseus arm. Since the distribution and number of star-forming regions beyond the Local arm remain poorly determined, these candidates present an opportunity to significantly improve our understanding of star formation within this distant spiral arm.

20264+4042 coincides with DR 7, and at an assumed distance of 7.5 kpc has an estimated luminosity of 360,000 $L_\odot$ corresponding to an O5.5 ZAMS star. The $^{12}$CO emission associated with this YSO appears at $V_{LSR} = -42.9$ km s$^{-1}$, consistent with membership in the Perseus arm, and is similar to the velocity obtained by Pipenbrink & Wendker (1988) for DR 7.

20144+3726 is located near the supernova remnant CTB 87 in a relatively isolated region mapped by Wendker (1984). The $^{12}$CO emission shows components only at $-57.2$ and $-71.5$ km s$^{-1}$ which are clearly in the velocity range for Perseus arm material. The $-57.2$ km s$^{-1}$ component shows the greatest correlation with the YSO's far-IR emission. At a distance of 10 kpc the luminosity of 20144+3726 is 26,000 $L_\odot$, equivalent to a single B0 ZAMS star. Since the thermal radio emission from such an SFR should have been detectable in the Wendker (1984) survey and was not, this YSO may be a prestellar object.

20321+4112 coincides with the peak of 18P61 identified by Landecker et al. (1989) as a Perseus arm SFR at a distance of 10 kpc. Our $^{12}$CO spectra only covered the velocity interval $\pm 35$ km s$^{-1}$ and show three distinct weak lines, of these the $-24.7$ km s$^{-1}$ component found to be variable in strength over the field, unlike the relatively constant brightness of the lower velocity features. Since Piepenbrink & Wendker (1988) were able to identify an $H_2CO$ line with $V_{LSR} = -64.6$ km s$^{-1}$ toward 18P61, the molecular emission corresponding to 20321+4112 was outside the bandpass for this $^{12}$CO survey.

We also identify 20327+4120 as a multiple-lined $^{12}$CO source with components at $-3$ and $-5.8$ km s$^{-1}$, and two weak lines near $-30$ km s$^{-1}$. The $-5.8$ km s$^{-1}$ line is associated with the YSO itself, implying that it is located within the Local arm. This YSO is situated in a relatively isolated field, with the nearest bright radio continuum peak, 18P61, located 10′ distant.

Although 20173+3714, 20332+4124 and 20290+4052 also have $^{12}$CO emission features at $V_{LSR} < -20$ km s$^{-1}$, these components are typically very weak, and their peak emission does not coincide with the *IRAS* position. For this reason we identify these as probable foreground Local arm SFRs observed against more distant Perseus arm molecular material.

The sharp drop in detected YSOs between $-35 < V_{LSR}$ (km s$^{-1}$) $< -10$ suggests that SFRs earlier than about B2 ZAMS (for $S[100\ \mu\text{m}] = 100$ Jy at a distance of 5 kpc) are absent in the Interarm Gap. This is consistent with the observations by Cohen et al. (1980) and Leung & Thaddeus (1992) which show that few large molecular clouds exist in this zone. We also note that in only seven directions out of the 70 sampled toward Cygnus X could emission from the Perseus arm be detected, implying that large molecular clouds of the kind present in the Local arm are comparatively less common.

The current survey of the YSO population in the Perseus Arm remains too sparse to determine the spatial extent of the young SFRs in this sector of the spiral arm. Deeper *IRAS* surveys for the more numerous low-luminosity YSOs in the Perseus arm should help to fill in the details of the spiral arm structure summarized in Figure 2 based on this initial study.

### 5.2. *Sources with No Detected* $^{12}$CO

Among the surveyed first-ranked YSO candidates were five (20099, 20103, 20324, 20406, and 20446) that had no detectable $J = 2$–1 emission to a limit of $T_R^* < 0.4$ K. As far-IR sources, they appear to be indistinguishable from the other sources in the survey both in terms of flux density and their degree of compactness as characterized by the *IRAS* Structure Coefficient. In Paper III we examined the Palomar Observatory Sky Survey (POSS) prints for these fields and found both individual faint stars (20099, 20103, and 20406) and nebulae (20324 and 20446) as candidate sources for the emission. Despite their brightness at 12 $\mu$m, however, these objects were not included in the Atlas so that additional data on their near-IR continua are not available.

20099 has the greatest discrepancy between the predicted and actual 12 $\mu$m emission based on the disk model discussed in § 4.3. The lack of detected $^{12}$CO emission confirms that this is not a typical YSO candidate. Its starlike appearance indicates that it is probably a late-type star rather than a YSO. 20103 and 20406 are probably also late-type stars with very large IR excesses.

20324 coincides with the eastern lobe of a bright but compact nebulosity only 20″ in extent. 20446 appears to be associated with a starlike object situated near the edge of a faint optical nebula approximately 40″ across.

Casoli et al. (1986) have also identified cold *IRAS* sources that resemble YSOs but that could not be detected in $^{13}$CO. The majority were among the weaker far-IR sources in their sample with $S(100\ \mu m) < 30$ Jy. This is in marked distinction to our survey where the undetected sources had $S(100\ \mu m) > 250$ Jy.

## 6. NEW OUTFLOW CANDIDATES

A variety of searches using the *IRAS* PSC have been undertaken over the years to identify new examples of YSOs with high-velocity outflows of cold molecular material (Heyer et al. 1987; Richards et al. 1987; Snell et al. 1988). In most cases, the distinction between an outflow-broadened spectral feature and one that is not is relatively straightforward, particularly when integrated wing maps confirm the characteristic "bipolar" appearance. The criteria most often used to identify outflows is a profile broadened by more than 10 km at $^{12}$CO ($J = 1$–0) which is also spatially confined to the YSO. Snell, Dickman, & Huang (1988) surveyed 22 *IRAS* sources with $S(100\ \mu m) > 500$ Jy and found six that met this criterion. Heyer et al. (1987), however, surveyed 30 *IRAS* sources with $S(100\ \mu m) > 10$ Jy and found only three YSOs whose wing maps showed clear evidence for outflows. The measured line widths at the 200 mK level in the profile, $\Delta V$(200 mK), among the three outflows were all typically $\approx 5.2$–7.4 km s$^{-1}$.

The YSOs toward Cygnus X that have been surveyed for $^{12}$CO emission may be conveniently grouped into two categories: (1) Objects with no evidence for broad wings or asymmetric line shapes which appear in Table 4, and (2) Objects with some evidence for broad, high-velocity wings or "pedestal" features which appear in Table 5. These tables list, where appropriate, the line center velocity $V_{LSR}$, peak line intensity, $T_R^*$, in K, the estimated line full width at zero intensity measured at the 500 mK level, $\Delta V$, integrated wing intensities, $I_{Red}$ and $I_{Blue}$ in K km s$^{-1}$, and pertinent comments on the spatial distributions of the line components and additional velocity components detected.

### 6.1. *Sources with No Broad Wings*

Many of the surveyed YSOs had readily detectable $^{12}$CO, but no clear indication of a high-velocity component. Tables 3 and 4 list 39 YSOs whose line profiles were not especially remarkable in width. Five of the members of this group, 20138, 20152, 20157, 20236, and 20286, are associated with unusually compact CO clouds described by Odenwald & Schwartz (1989, hereafter Paper IV), and for which line emission could be clearly detected only within a few arcminutes of the *IRAS* position. The corresponding optical images show dark globules or optical nebulae 1′–2′ (0.3–0.6 pc) in size with $M < 25\ M_\odot$.

The spectra of the remaining sources in Tables 3 and 4 often show a prominent $^{12}$CO ($J = 2$–1) line within the 3′ × 3′ map present throughout the field, but brightest at the *IRAS* position, suggesting that the *IRAS* sources are probably associated with molecular clouds whose sizes exceed the mapped areas.

20261 is significantly offset from the broad peak of DR 6, and has an equivalent spectral type of about B3 ZAMS at a distance of 1.5 kpc (Paper I). 20293 and 20343 coincide with DR 15:FIR 2 and DR 20/FIR 5 decribed in Paper II, and whose far-IR luminosity is equivalent to young O9.5 and B2.5 ZAMS stars at a distance of 1 kpc. 20300 is coincident with DR 13, and for a distance of 1.5 kpc (Landecker et al. (1989) has a luminosity equivalent to an O6 ZAMS star.

### 6.2. *Broad Wing Sources and Outflow Candidates*

The 21 objects listed in Table 5, in addition to 20160 and 20219 in Table 3, all showed line emission with a broad component for which $\Delta V(500\ \text{mK}) > 5.0$ km s$^{-1}$. Included among them are the already well-studied sources S 106 (20255) and AFGL 2591 (20275), along with 20188 described by Little et al. (1988). 20220, associated with the radio source 18P26, has a strong blue wing detected at nearly all mapped positions and is one of the brightest sources in the survey. Assuming a distance of $\approx 2$ kpc, its estimated spectral type is O5 ZAMS. It is located near ON 2 and Cyg OB1 and was mapped by Casoli et al. (1986). 20306+4005 whose assumed distance is 1 kpc (Paper II) has an estimated spectral type of $\approx$O7 ZAMS. Located near DR 15 (18P59) and AFGL 2602, it has $^{12}$CO emission that varies in brightness in a complex manner over the field surveyed; however, the component at $V_{LSR} = +3.9$ km s$^{-1}$ shows a broad red wing and is probably the associated outflow source.

Among the candidates whose estimated far-IR luminosities are in the range from B1 to B0.5 ZAMS were 20255, 20275, 20277, 20332, and 20333. 20277 near DR 9 has broad-line emission at a position 1′ south and west of the *IRAS* position, suggesting that more extensive mapping is needed. 20332 is an isolated source whose strongest $^{12}$CO line emission occurs near $V_{LSR} = -1.3$ km s$^{-1}$, consistent with an Local arm distance assignment. The $^{12}$CO emission from 20333 near DR 18 was not detected at all positions; however, it was found to be strongest and broadest near the *IRAS* position.

The remaining YSO candidates listed in Tables 3 and 5 had estimated luminosities in the B2–B3 ZAMS range, assuming distances of 2 kpc. With the possible exception of 20215 near 18P26, none coincide with bright, compact radio peaks, suggesting that their intrinsic ionization rates are probably insufficient to support strong H II regions as befits their, apparently, late spectral classification. Some of these may include candidates for very young stellar objects that have not yet begun

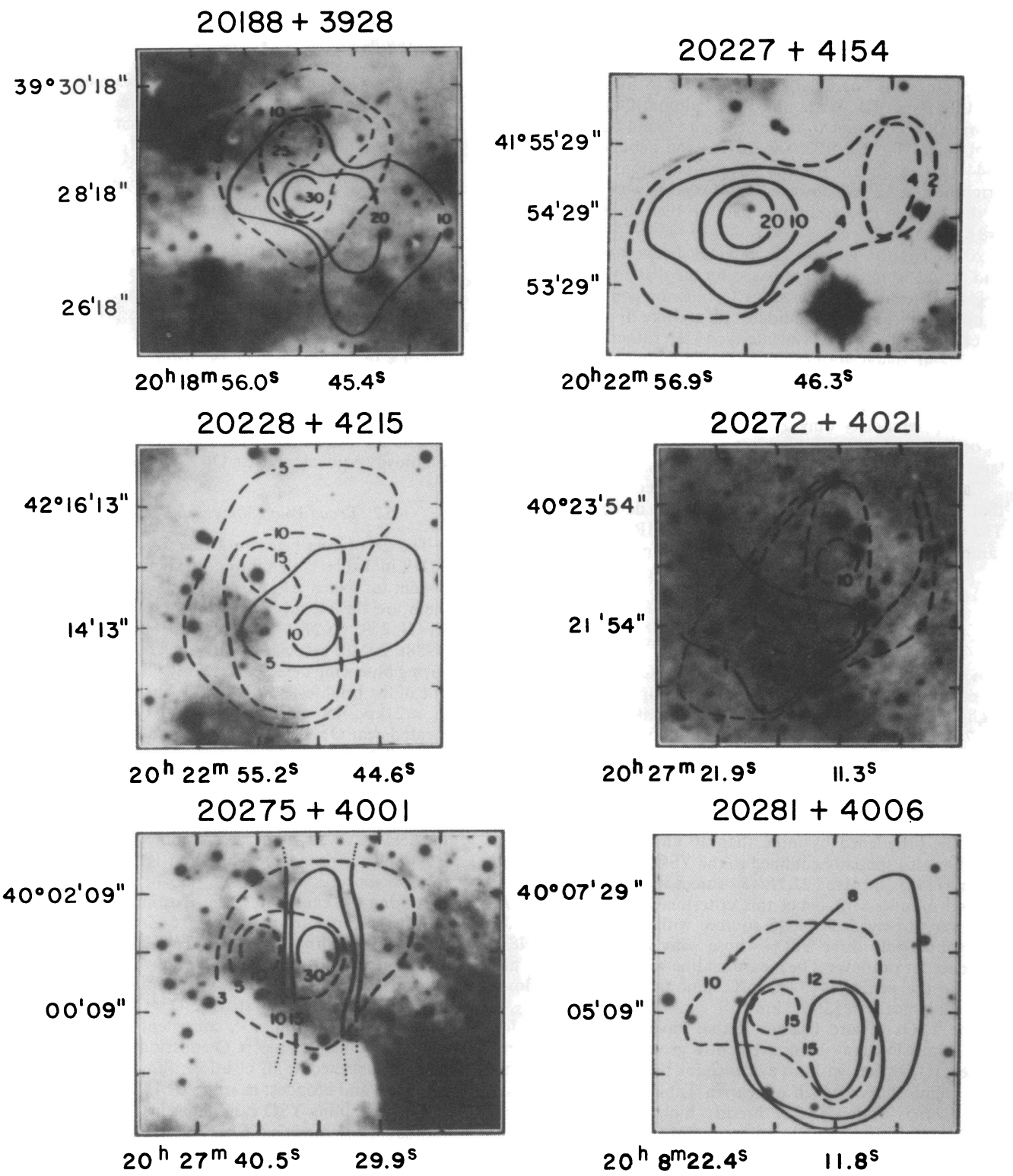


FIG. 7.—Wing maps of selected YSOs with the strongest high-velocity molecular outflow emission. Red wing emission is indicated by dashed contours; blue wings are indicated with solid contour lines. The contour steps are in units of K km s$^{-1}$ in the $^{12}$CO ($J$ = 2–1) transition.

to produce significant photoionizing radiation from their photospheres.

An important secondary characteristic of many outflow sources is the spatially offset distributions of their "red" and "blue" wing components. Sufficient spectral data exist for the broad-wing sources in this survey to create wing maps displaying the spatial distribution of the high-velocity line emission. Most of the sources in Table 5 had unmistakably broad wings; however, the 3 × 3 grid was often too small to determine the true extent of the emission. In Figure 7 the maps of the strongest broad-line sources are shown, superposed on POSS "red" photographs of each region. Of these, only 20188, previously mapped by Little et al. (1988), had anything like a classical bipolar shape. The YSOs all coincide with fields containing significant optical extinction.

Including the known outflow sources S 106, AFGL 2591, and 20188, the current, flux-limited survey has identified, at most, 24 broad-winged, outflow candidates from among a total sample of 70 YSOs surveyed with $S(100\ \mu m) > 100$ Jy. If we discount the five objects that could not be detected in $^{12}CO$ ($J = 2$–1), the detection rate for high-luminosity outflows toward Cygnus is 39% ± 9%. This is similar to the 29% ± 8% cited by Schwartz et al. (1990) in their survey of low-luminosity YSOs in nearby molecular clouds. Our results are also similar to those of Snell et al. (1990) who found that half of the *IRAS* sources with $S(100\ \mu m) > 500$ Jy had associated outflows. Our survey, contains 25 sources in this flux density range, of which no more than 12 had broad wings.

## 7. CONCLUSIONS

We have identified 70 YSO candidates in the Cygnus X region with equivalent luminosities earlier than A0 ($d > 700$ pc) or B4 ($d > 2000$ pc). Our $^{12}CO$ survey shows that nearly all of the bright YSO candidates are associated with the Local arm population based on their line velocities. We have detected a new SFR in the Perseus arm, 20114+3726, with an estimated spectral type of B0 ZAMS. Based on this flux limited survey, we conclude that in the direction of Cygnus X all of the YSOs in the Perseus arm earlier than B0 ZAMS have now been identified.

From the $^{12}CO$ data, we have also detected 23 broad-line YSOs; three of these are the known outflow sources S 106, RAFGL 2591, and 20188. An additional 10 YSOs have wing maps that show a complex distribution of high-velocity material, often with a linear or polar geometry.

Future $^{12}CO$ observations of the remaining faint YSO candidates will complete the survey for low-luminosity SFRs toward Cygnus to anticipated luminosity limits of A0 ZAMS in the Local arm, and B5 ZAMS in the Perseus arm, and clarify the location and extent of both the Perseus arm and the Interarm Gap as traced by SFRs.

## REFERENCES


Abbott, D. C., Bieging, J. H., & Churchwell, E. 1981, ApJ, 250, 645
Alter, G., Balazs, B., & Ruprecht, J. 1970, Catalog of Star Clusters and Associations (Budapest: Akademiai Kiado)
Atlas of Low Resolution *IRAS* Spectra. 1986, *IRAS* Science Team, prepared by F. M. Olnon & E. Raimund, A&AS, 5, 607
Baars, W. M., & Wendker, H. J. 1981, A&A, 101, 39
Barcia, A., et al. 1985, A&A, 147, 237
Beckwith, S. V. W., Sargent, A. I., Chini, R. S., & Guster, R. 1990, AJ, 99, 924
Beuermann, K., Kanbach, G., & Berkhuijsen, E. M. 1985, A&A, 153, 17
Bloemen, H. 1987, in Interstellar Processes, ed. D. J. Hollenbach & H. A. Thronson, Jr. (Dordrecht: Reidel), 143
Bochkarev, N. G., & Sitnik, T. G. 1985, Ap&SS, 108, 237
Burton, W. B. 1985, A&AS, 62, 365
———. 1988, in Galactic and Extragalactic Radio Astronomy, ed. G. L. Verschuur & K. I. Kellerman (New York: Springer), 295
Campbell, M. F., Hoffmann, W. F., & Thronson, H. A. 1981, ApJ, 247, 530
Campbell, M. F., Hoffmann, W. F., Thronson, H. A., & Harvey, P. M. 1980, ApJ, 238, 122
Cash, W., Charles, P., Bowyer, S., Walker, F., Garmire, G., & Riegler, G. 1980, ApJ, 238, L71
Casoli, F., Dupraz, C., Gerin, M., Combes, F., & Boulanger, F. 1986, A&A, 169, 281
Cohen, R. S., Cong, H., Dame, T. M., & Thaddeus, P. 1980, ApJ, 239, L53
Cong, H. 1977, Ph.D. thesis, Columbia Univ.
Dame, T. M., et al. 1987, ApJ, 322, 706
Davies, R. D. 1957, MNRAS, 117, 633
Dickel, H. R., & Wendker, H. J. 1978, A&A, 66, 289
Dickel, H. R., Wendker, H. J., & Bieritz, J. H. 1969, A&A, 1, 270
———. 1970, in IAU Symp. 38, The Spiral Structure of our Galaxy, ed. W. Becker & G. Contopoulos (Dordrecht: Reidel), 213
Downes, D., & Rinehart, R. 1966, ApJ, 144, 937
Elsasser, H., & Voelcker, K. 1974, in H II Regions and the Galactic Center, 8th ESLAB Symp., ed. A. F. M. Moorwood (ESRO/STIB: Noordwijk), 195
Georgelin, Y. P., & Georgelin, Y. M. 1976, A&A, 49, 57
Habing, H. J. 1986, in The Galaxy, ed. G. Gilmore & R. Caswell (Dordrecht: Reidel), 173
Habing, H. J. 1987, in IAU Symp. No. 122, Circumstellar Matter, ed. I. Appenzeler & C. Jordan (Dordrecht: Reidel), 207
Hauser, M. 1990, in After the First Three Minutes, ed. S. Holt, C. Bennett, & V. Trimble (New York: AIP), 161
Hauser, M. G., et al. 1984, ApJ, 285, 74
Heske, A., & Wendker, H. J. 1985, A&A, 148, 439
Heyer, M. H., Snell, R. L., Goldsmith, P. F., & Myers, P. C. 1987, ApJ, 321, 370
Hoffmann, W. F., Frederick, C. L., & Emery, R. J. 1971, ApJ, 170, L89
Huchtmeier, W. K., & Wendker, H. J. 1977, A&A, 58, 197
Humphreys, R. 1976, PASP, 88, 647
*IRAS* Point Source Catalog, Version 2.0. 1988, Joint *IRAS* Science Working Group (Washington: GPO)
*IRAS* Catalogs and Atlases: Explanatory Supplement. 1988, ed. C. A. Beichmann, G. Neugebauer, H. J. Habing, P. E. Clegg, & T. J. Chester (Washington: GPO)
Landecker, T. L., Wendker, H., & Higgs, L. A. 1989, J. Roy. Astron. Soc. Canada, 83, 315
Leung, H. O., & Thaddeus, P. 1992, ApJS, 81, 267
Liszt, H. S. 1985, in IAU Symp. 106, The Milky Way Galaxy, ed. H. van Woerden, R. Allen, & W. Burton (Dordrecht: Reidel), 283
Little, L. T., Bergman, P., Cunningham, C., Heaton, B., Knee, L., MacDonald, G., Richards, P., & Toriseva, M. 1988, A&A, 205, 129
Magnani, L., Blitz, L., & Mundy, L. 1985, ApJ, 295, 402
Natta, A., & Panagia, N. 1977, A&A, 50, 191
Neckel, T., & Klare, G. 1980, A&AS, 42, 251
Odenwald, S. F. 1989, AJ, 97, 801 (Paper III)
Odenwald, S. F., & Schwartz, P. R. 1989, ApJ, 345, L47 (Paper IV)
Odenwald, S., Schivanandan, K., Campbell, M., Fazio, G., Schwartz, P., & Moseley, H. 1986, ApJ, 306, 122 (Paper I)
———. 1990, AJ, 99, 288 (Paper II)
Olnon, F. M., Bavel, B., Habing, H. J., De Jong, T., Harris, S., & Pottasch, S. R. 1984, ApJ, 278, L41
Panagia, N. 1972, AJ, 78, 929
Piddington, J. H., & Minnett, H. C. 1952, Australian J. Sci. Res. A, 5, 17
Piepenbrink, A., & Wendker, H. J. 1988, A&A, 191, 313
Reddish, V. C. 1967, MNRAS, 135, 251
Reddish, V. C., Lawrence, L. C., & Pratt, N. M. 1966, Publ. Roy. Obs. Edinburgh, 5, 111
Reifenstein, E. C., Wilson, T. L., Burke, B. F., Mezger, P. G., & Altenhoff, W. J. 1970, A&A, 4, 357
Ressler, M. E. 1992, BAAS, 23, 1446
Richards, P. J., Little, L. T., Toriseva, M., & Heaton, B. D. 1987, MNRAS, 201, 121
Schmidt-Kaler, Th. 1976, Vistas Astron., 19, 69
———. 1971, in Structure and Evolution of the Galaxy, ed. L. N. Mavridis (Dordrecht: Reidel), 93
Schwartz, P. R., Gee, G., & Huang, Y.-L. 1988, ApJ, 327, 350
Schwartz, P. R., Mozurkewich, D., & Odenwald, S. F. 1990, in preparation
Shu, F., Adams, F. C., & Lizano, S. 1987, ARA&A, 25, 23
Simonson, S. C. 1974, A&A, 46, 261
Snell, R., Dickman, R., & Huang, Y. 1990, ApJ, 352, 139
Verter, F., & Rickard, L. J. 1992, in preparation
Wendker, H. J. 1970, A&A, 4, 378
———. 1984, A&AS, 58, 291
Wendker, H. J., Benz, D., & Baars, J. W. M. 1983, A&A, 124, 116
Zoonematkermani, S., Helfand, D. J., Becker, R. H., White, R. L., & Perley, R. A. 1990, ApJS, 74, 181
Zuckerman, B., & Dyck, H. M. 1986, ApJ, 304, 394
Zuckerman, B., Dyck, H. M., & Claussen, M. J. 1986, ApJ, 304, 401